EU contribution to the test and analysis of the ITER poloidal field conductor insert and the central solenoid model coil



2009 Supercond. Sci. Technol. 22 085006

(http://iopscience.iop.org/0953-2048/22/8/085006)

Supercond. Sci. Technol. **22** (2009) 085006 (11pp) doi:10.1088/0953-2048/22/8/085006

# EU contribution to the test and analysis of the ITER poloidal field conductor insert and the central solenoid model coil

**R Zanino[1,6], M Bagnasco[2], D Ciazynski[3], B Lacroix[3], E P A van Lanen[4], S Nicollet[3], A Nijhuis[4], L Savoldi Richard[1], C Sborchia[5], A Torre[3], A Vostner[5] and L Zani[3]**

[1] Dipartimento di Energetica, Politecnico di Torino, I-10129 Torino, Italy
[2] EPFL-CRPP, CH-5232 Villigen PSI, Switzerland
[3] CEA, IRFM, F-13108 Saint-Paul-lez-Durance, France
[4] University of Twente, 7500 AE Enschede, The Netherlands
[5] F4E, 08019 Barcelona, Spain

E-mail: roberto.zanino@polito.it

Received 26 April 2009, in final form 3 June 2009
Published 15 July 2009
Online at stacks.iop.org/SUST/22/085006

**Abstract**
The PFCI is a single-layer solenoid wound from a 45 m long ITER-type NbTi dual-channel cable-in-conduit conductor, designed to be representative of the one currently proposed for the ITER PF1&6 coils. The PFCI, installed in the bore of the ITER central solenoid model coil (CSMC) at JAEA Naka, Japan, and well instrumented from both the thermal hydraulic and the electromagnetic points of view, has been successfully tested in June–August 2008. The test concentrated on DC performance (current sharing temperature and critical current measurements) and AC loss measurements. The results of the analysis of those measurements are reported in the paper, with particular attention to the comparison with the PFCI short sample, which was previously tested in the SULTAN facility. The evolution of the DC performance of the CSMC is also discussed.

(Some figures in this article are in colour only in the electronic version)

## 1. Introduction

The poloidal field conductor insert (PFCI) is the last in a series of model and insert coils tested within the International Thermonuclear Experimental Reactor (ITER) R&D framework from the year 2000 on [1–5], and the first one using NbTi. Since they operate in low magnetic field ($\leqslant$6 T), the ITER poloidal field (PF) coils will use NbTi, instead of Nb3Sn, as the central solenoid and toroidal field coils, thus reducing the cost of fabrication [6]. The PFCI is a single-layer solenoid, see figure 1(a), wound from a 45 m long ITER-type NbTi dual-channel cable-in-conduit conductor (CICC), see figure 1(b), representative of the one currently proposed for the ITER PF1&6 coils [7]. An intermediate joint (IJ) connects the main winding to a second piece of the same conductor, which is called the upper busbar, see figure 1(a). The IJ was included in the winding in order to test an overlap shaking-hand joint as foreseen in the ITER PF coils, under the PF operating conditions (i.e. axial and radial magnetic field variations). The PFCI main winding and upper busbar are cooled by two separate hydraulic circuits using supercritical helium at nominal 4.5 K and 0.5 MPa inlet conditions.

The PFCI was fabricated by Tesla Engineering, UK, starting from a cable produced in Russia by VNIIM/VNIIKP and jacketed at ASG Superconductors, Italy [8]. Like its predecessors, it was installed in the bore of the ITER central solenoid model coil (CSMC) at JAEA Naka, Japan [9], see figure 1(c). The PFCI instrumentation included thermometers along the conductor, flow meters, pressure taps and different heaters on the inlet piping, conductor and IJ, see figure 1(a), as well as a series of voltage taps located along and around the main winding, together with pick-up (PU) coils close to the main winding and IJ for magnetization measurements [10]. The CSMC provides the nominal background field of 6 T,

[6] Author to whom any correspondence should be addressed.

 

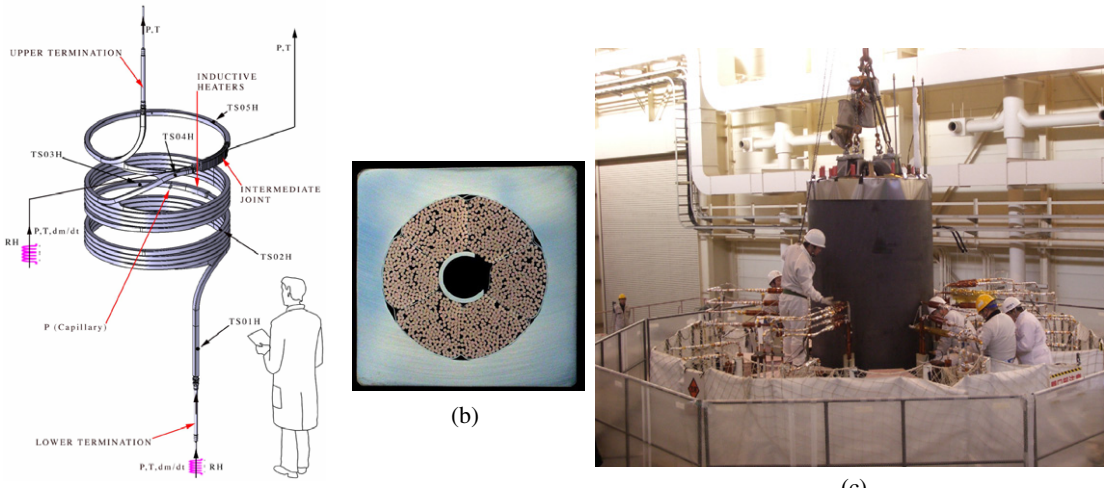


**Figure 1.** (a) Sketch of the PFCI with some instrumentation. (b) Cross section of the PFCI CICC (square SS jacket side $\sim$ 50.3 mm). (c) The PFCI being inserted in the CSMC bore at JAEA Naka in early 2008.

whereas the nominal operating current of 45 kA adds a non-negligible self-field contribution, leading to a significant field variation ($\sim$1 T) over the cross section of the conductor, similar to that in the ITER PF coils.

As for other insert and model coils, a short NbTi sample (PFCI-FSJS) made with the same conductor was tested before the PFCI, in 2004, in the SULTAN facility at Villigen PSI, Switzerland [11, 12]. The results of these tests were not fully satisfactory from the point of view of the DC performance, as sudden quenches (i.e. without a smooth voltage transition, at least at the level detectable with the available diagnostics set-up[7]) occurred prematurely whenever the transport current $I$ was above a certain threshold, resulting in a quench current well below the value $I_C^{peak} \equiv [I_C^{strand}(B_{peak}^{max}) \times (\#\text{ of strands})]$, which was the minimum expected $I_C$ from single-strand performance (here $I_C^{strand}(B_{peak}^{max})$ is the measured critical current of the strand evaluated at the maximum peak field seen by any strand in the CICC). The sudden occurrence of the quench has to do with the large magnetic field gradient on the cross section (at large $I$) combined with the large $|\partial j_C/\partial B|$ and $n$ peculiar to NbTi ($j_C$ being the critical current density of the superconductor and $n$ being the exponent of the empirical power law relation between electric field and current density), resulting in an (average) electric field at the quench smaller than the critical field $E_C$ (conventionally set at 10 $\mu$V m$^{-1}$); the premature appearance of the quench can be explained by a non-uniformity of the current distribution on the conductor cross section. While the short sample performance was considered sufficient for the ITER PF coils after a design review [13], it was obviously of principal importance to verify if the long length at peak field and longer distance between the joint and peak field peculiar to the PFCI versus the PFCI-FSJS could improve the current distribution in the most critical conductor region and, as a consequence, the performance of the PFCI with respect to that of the PFCI-FSJS.

The PFCI was tested for about two months in 2008. While the main test results are summarized in [7], this paper will concentrate on the analysis of the two major items of the test, namely:

- analysis of current sharing temperature ($T_{CS}$) and critical current ($I_C$) measurements, using available conductor models in the different EU laboratories;
- analysis of AC losses in the main winding and in the IJ, including an estimate of the error bar.

Preliminary results of the analysis of these two test items were presented in [14].

Additional items of the test discussed in this paper include the resistance of, and heat transfer in, the IJ and ramp-rate limitation (RRL). Stability and quench tests were also included in the test program but their analysis will be reported elsewhere. Finally, as is customary in all previous tests of ITER insert coils, the DC performance of the CSMC 1A conductor was also re-tested, in a single reference scenario, and the results will be reported here.

The results of the PFCI test improved on the reduced performance shown by the PFCI short sample and more generally provide a significant database for the ITER PF coils. In particular, the tests confirmed that:

- the quench current was higher in the PFCI than in the PFCI-FSJS. While sudden quenches still occur above a certain current threshold, because of the comparable self-field gradient on the CICC cross section, the PFCI could operate in DC conditions with no premature quenches with respect to its strand at peak magnetic field, as opposed to the case of its short sample—an indirect indication of improved current uniformity at maximum field along the conductor length.

[7] As the measured voltage is related to the weighted average (on the cable cross section) of the electric field developed on the different cable elements, and integrated between the voltage taps, any transition should be seen starting smooth by ideal voltage taps, since at the single-strand level the transition is obviously smooth. However, a fast electric field increase, associated with a fast uncontrolled temperature increase at the strand level, is seen as a sudden quench by the available diagnostics [12].

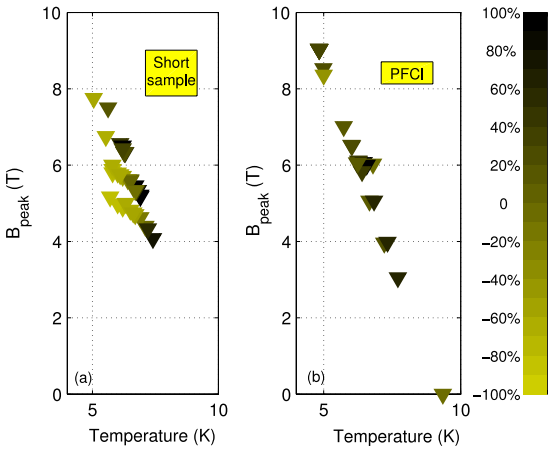


**Figure 2.** Summary of DC performance: (a) short sample (data from [11]) and (b) PFCI (data from [7]). The relative deviation $(I_{C,quench} - I_C^{peak})/I_C^{peak}$ between the measured critical or quench current and that resulting from all strands carrying the $I_C$ at maximum peak field is reported in the scale on the right. Lighter triangles imply degradation.

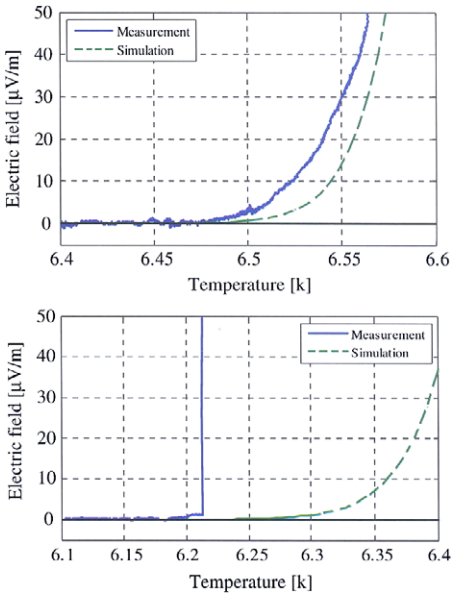


**Figure 3.** Evolution of measured and computed (JackPot) voltage in the case of two $T_{CS}$ tests vs. T03H signal: (top) run 53-01, $I_{PFCI} = 6$ kA and $B_{CSMC} = 5.9$ T (bottom) run 35-01, $I_{PFCI} = 55$ kA and $B_{CSMC} = 5.15$ T.

- the resistance of the IJ (and lower termination) was much lower than in the case of the short sample thanks to improved manufacturing: the result of the electrical measurement [7] was confirmed calorimetrically, see below.
- the AC losses in the PFCI main winding follow the similar monotonically increasing trend with cycling as measured on the Twente press after ∼100 cycles.
- some degradation was observed in the PFCI conductor performance at the maximum ramp rate allowed by the test set-up, see below, as well as in the IJ DC performance [7].

## 2. DC performance

The criterion for defining $I_C$ and $T_{CS}$ is an average electric field (on the cable cross section) $E = E_C$, which is deduced by dividing the measured voltage by the distance of the respective voltage taps.

The results of both $T_{CS}$ and $I_C$ tests of the PFCI (undistinguished, since they lead to essentially identical results) are summarized in figure 2, where they are reported in the form of relative deviation of $I_{C,quench} \equiv \min\{I_C, I_{quench}\}$ with respect to the collective strand-like behavior at the maximum peak magnetic field, i.e. with respect to $I_C^{peak}$, and compared to the short-sample results.

All results are given as a function of measured (jacket) temperature in the high field region and *peak* magnetic field. We see that for the PFCI, typically, the relative deviations are positive, i.e. $I_{C,quench} \geqslant I_C^{peak}$ (large positive relative deviations being an artifact of the small denominator $I_C^{peak}$ in the case of small currents, or of the large $|\partial j_C/\partial T|$); in contrast, the short sample also shows significant negative deviations (i.e. degradation). Both the PFCI and the short sample exhibit limiting currents, above which no critical current (smooth transition), strictly speaking, can be measured, but their performance is different above this limiting current. Whereas the strand itself is stable at the peak field value, when tested on a barrel, in the PFCI $T_{CS}$ and $I_C$ tests, both smooth and sudden transitions occurred, depending on the current level: as an example, it can be seen in figure 3 that the transition was smooth at 'low' current but sudden (within the accuracy/resolution of the available diagnostics, see above) at 'high' current, which is a common feature of both the PFCI and the short sample [11, 15]. Both the strand-like performance (in the case of uniform current distribution) and the smooth versus sudden transition at low versus high currents were anticipated by the predictive simulations [16].

In order to analyze this phenomenon, a classical approach can be followed as a first approximation, by assuming a uniform current distribution among all strands, then computing the average electric field across the cable cross section using the magnetic field map, the measured strand critical current and $n$ value [17]. Two runs (25-1 and 45-1) have been checked following this approach, one at high current (45 kA) and the other at low current (18 kA). The computed $T_{CS}$ is ∼6.4 K and ∼6.5 K, respectively, i.e. within 0.1 K from the measured $T_{CS}$ in run 45-1 and $T_{quench}$ in run 25-1. These deviations could be related to a possible current distribution imbalance, to temperature gradients (ignored in the model) and/or to thermometer accuracy. The major conclusion here is that if we compute $T_{CS}$ for a uniform current distribution we should find a somewhat higher $T_{CS}$ than the strand at peak field and therefore higher than in the experiment (e.g. due to current non-uniformity).

If we relax the assumption on uniform current distribution, the recently developed model JackPot [18], accounting for the precise strand trajectories in the spatially varying magnetic field, substantiates why there can be an important difference in performance between the test of a short sample and a coil,

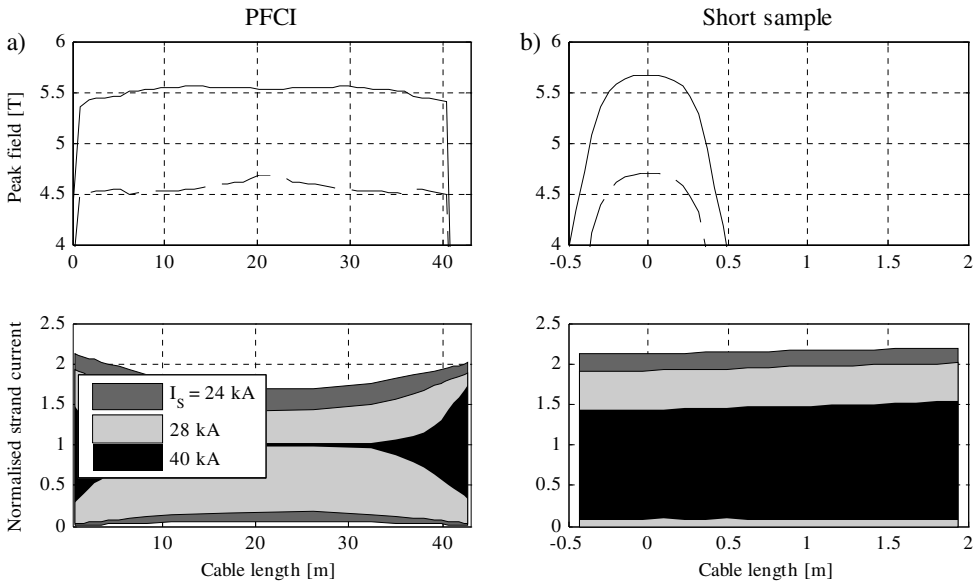


**Figure 4.** Profiles computed with JackPot along the cable length. (a) Top: maximum (solid line) and minimum (dashed line) magnetic field on the CICC cross section for $I = 40$ kA; bottom: strand current distribution (normalized with respect to the average), for different cable currents. The cable length is measured from the IJ hydraulic inlet, implying that the IJ is on the left side (small value of the abscissa) while the bottom termination is on the right. (b) Same as (a), but now for the PFCI-FSJS (short sample). In this case, the cable length is measured from the joint hydraulic outlet, implying that the bottom joint is on the left while the upper termination is on the right.

in particular for high currents. The model demonstrates that the disturbing influence of the joints on the test results, as observed earlier on a short sample of a similar PF cable and attributed to a combination of non-uniformity and local peak voltages [11], is practically negligible in the case of the PFCI. The relatively large non-uniformity in the short-sample test has been confirmed by transverse voltage measurements and Hall sensor array analysis [19]. A good assessment of the coil requires *a priori* the ability for sufficiently homogeneous current distribution among the strands in the high field region, and this condition is indeed reached in the PFCI, see [18]. Only near the joints does the current distribution remain inhomogeneous beyond this level (see figure 4(a)), but since the magnetic field in this region is sufficiently low, this does not affect the overall coil performance in a serious way [18]. Two $T_{CS}$ runs (35-1 and 53-1) were simulated with JackPot and compared with the signal from VD_0910, see figure 3, against the temperature measured at T03H with correction for magnetic field dependence, see [14]. At low current (upper plot in figure 3), the simulation, based on measured strand [17] and PFCI-FSJS joint properties, matches very well with the measurement, with a difference of only 20 mK. At high current (lower plot in figure 3), the start of a smooth transition is visible, but rapidly evolves into a sudden quench, before the electric field builds up the 10 $\mu$V m$^{-1}$ value. The take-off appears ~0.15 K later in the simulation, which assumes a constant and homogeneous temperature distribution in the cable and does not take into account the detailed dynamics of a quench; more specific analysis on this behavior is still ongoing. Apparently, the transition processes in the cable at low and high currents are different, and likely under the influence of the large cable self-field gradient, possibly in combination with the current non-uniformity. From that point of view, a slight underperformance compared to the single-strand properties is not surprising.

Figure 4(b) shows a simulation of a short sample with the same settings as the PFCI (same joint and cable properties, a peak field of 5.5 T and a temperature of 7.3 K). It appears that, mainly due to its short length, the sample is unable to redistribute the current as well as the PFCI does. As a result, a number of strands are overloaded in the high field region of the PFCI-FSJS, whereas the current is almost uniformly distributed in the high field region of the PFCI. According to the JackPot simulations, this is the explanation for the much better performance of the PFCI, when compared to the PFCI-FSJS.

## 3. Ramp-rate limitation

There have been two occurrences of an early quench at 5 kA s$^{-1}$ which can be interpreted as a ramp-rate limitation of the PFCI. The operating conditions of those two runs are compiled in table 1. Except for the 0.7 K difference in temperature, all other parameters are quite similar. The analysis of the measured signals reveals that, for both runs, the voltage which shows early signs of abnormal activity is VT56, located in the high field region. This voltage increases ~1.3 s before quench detection in run 148-1, and is already saturating the acquisition channel during the plateau of run 58-1. Indeed, the worst conditions for the conductor in run 58-1 are reached at the end of the ramp-up. Furthermore, the pick-up coils signals did not reveal any abnormal activity in the IJ during those early quenches, thus excluding a quench initiation in the IJ.

Hence, it seems correct to conclude that, for both runs, the quench initiated in the high field region during ramp-up, at

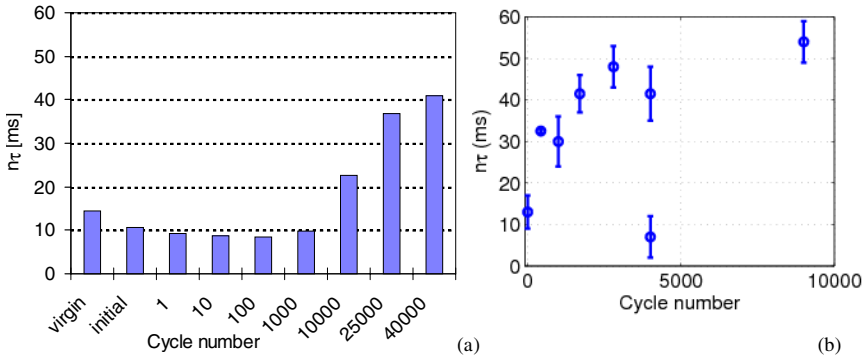


**Figure 5.** (a) Measured conductor loss time constant in the short PFCI sample tested in the Twente press at zero load (from [20]); (b) calorimetrically assessed time constant for the PFCI in the case of 4 T exponential coil dumps.

**Table 1.** Operating conditions and static properties of the conductor.

| Run # | 148-1 | 58-1 |
|---|---|---|
| Nature of the test | Ramp-rate test | Cyclic test |
| $I_{\mathrm{CSMC}}$ (kA) | 29.06 | 29.16 |
| $I_{\mathrm{PFI\ max}}$ (kA) | 37.06 | 30 |
| $B_{\mathrm{max}}$ (T) | 8.38 | 8.30 |
| $\mathrm{d}I/\mathrm{d}t$ (kA s$^{-1}$) | 5 | 5 |
| $T = (T_{\mathrm{IN}} + T_{\mathrm{OUT}})/2$ (K) | 5.01 | 4.32 |
| Quench detection | During ramp-up | During ramp-down |
| Static $T_{\mathrm{CS}}@I_{\mathrm{op}}$ (K) | 5.29 | 5.27 |
| Static $I_{\mathrm{C}}@T_{\mathrm{op}}$ (kA) | 51.2 | 165.7 |

$I_{\mathrm{PFCI}} \sim 30$ kA. When comparing these pulsed conditions with the static properties of the conductor, we find that run 148-1 shows a medium degradation of the performances ($\sim$0.3 K) while run 58-1 shows a drastic deviation ($\sim$1 K reduction) from the conductor's static behavior.

## 4. AC losses

AC losses were measured on both the conductor and the IJ using different test scenarios (exponential, trapezoidal, etc) as well as in different phases of the tests (i.e. before, during and after completing a series of about 9000 full loading cycles) [7]. The results of the conductor measurement are translated below into a (single) characteristic coupling time constant $n\tau$, as is customary (more sophisticated models include multiple time constants [22] or account for Lorentz load and cycling [23] based on the press measurements from [20], but they are beyond the scope of the present paper). The PFCI test results can then be compared with the measurement results from a PFCI conductor short sample tested in the Twente press [20] and/or from sub-size NbTi conductors tested in SULTAN [21]. The AC loss measured in the Twente press showed an initial decrease from the virgin state value ($\sim$15 ms) down to $\sim$10 ms, followed then by a monotonic increase to $\sim$30 ms after 10 000 cycles and $\sim$50 ms after 40 000 cycles (exact values depending also on the load conditions), see figure 5(a).

As opposed to this, an earlier saturation of the loss was observed in SULTAN tests of sub-size NbTi samples. Below we describe the results of our analysis of the PFCI losses, with particular reference to the calorimetric assessment of both conductor and IJ losses following 4 T dumps of the CSMC performed at different stages during the whole PFCI test campaign.

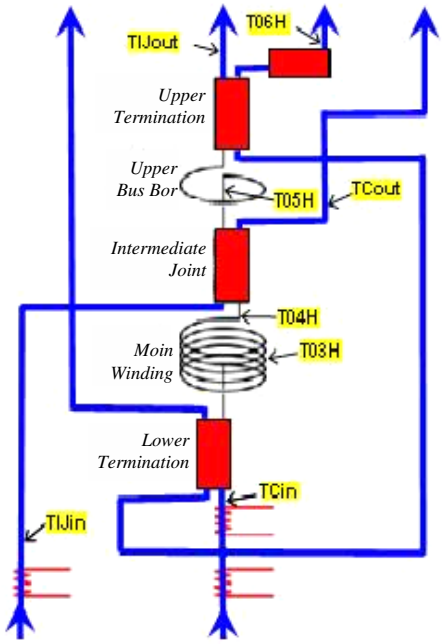


**Figure 6.** Sketch of the hydraulic circuits relevant for PFCI calorimetry.

### 4.1. Calorimetric evaluation of conductor and IJ losses

The assessment of the AC loss is in principle straightforward, but very delicate in practice. With reference to figure 6 we may note that steady state 0D energy balances can be written separately for the main winding[8], the IJ and the upper busbar,

[8] Other choices of thermometers are available in principle for the assessment of $Q_{\mathrm{WIND}}$, namely the pairs (TCin, T03H), giving the loss in the lower half of the main winding, and (T03H, T04H), giving the loss in the upper half of the main winding, both of which could be assumed to be $\sim Q_{\mathrm{WIND}}/2$. However, these alternative choices were not used because the corresponding variation $|\Delta h_{\mathrm{initial}} - \Delta h_{\mathrm{final}}|$ is larger (compare 45 J kg$^{-1}$ when T04H and TCin are used, with, for example, $\sim$65 J kg$^{-1}$ if T04H and T03H are used, see figure 7).

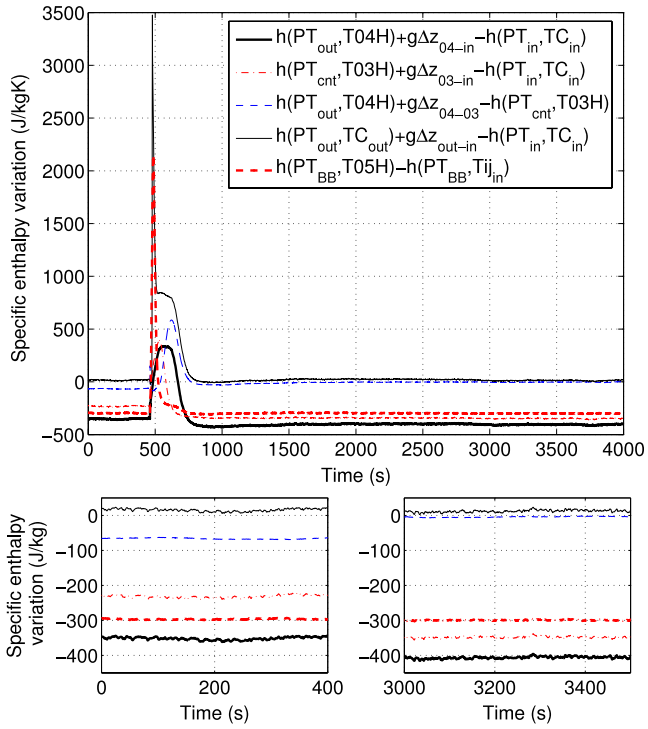


**Figure 7.** Evolution of measured enthalpy differences of relevance for the calorimetric assessment of AC losses. Case of run 74-02.

respectively, as follows:

$$Q_{\mathrm{WIND}} = (\mathrm{d}m/\mathrm{d}t)_{\mathrm{cond}}[h(\mathrm{PT\_out, T04H}) - h(\mathrm{PT\_in, TCin}) + g\Delta z_{04-\mathrm{in}}]$$

$$Q_{\mathrm{IJ}} = (\mathrm{d}m/\mathrm{d}t)_{\mathrm{cond}}[h(\mathrm{PT\_out, TCout}) - h(\mathrm{PT\_out, T04H})] + (\mathrm{d}m/\mathrm{d}t)_{\mathrm{bus}}[h(\mathrm{PT\_BB, T05H}) - h(\mathrm{PT\_BB, TIJin})]$$

$$Q_{\mathrm{BUS}} = (\mathrm{d}m/\mathrm{d}t)_{\mathrm{bus}}[h(\mathrm{PT\_BB, TIJout}) - h(\mathrm{PT\_BB, T05H})] + (\mathrm{d}m/\mathrm{d}t)_{\mathrm{IPI}}[h(\mathrm{PT\_in, T06H}) - h(\mathrm{PT\_in, TCin})]$$

where the single terms have the dimensions of a power (W), $\mathrm{d}m/\mathrm{d}t$ is the mass flow rate, $h$ is the He enthalpy, all pressures and temperatures being measured functions of time; $g\Delta z$ is the contribution of potential energy (not included in [14]), which is non-negligible in view of the elevation difference between pressure taps at the inlet and outlet of the main winding (whereas it is negligible between the inlet and outlet of IJ and busbar, and therefore not included in $Q_{\mathrm{IJ}}$ and $Q_{\mathrm{BUS}}$). $Q_{\mathrm{WIND}}$, strictly speaking, includes the loss in the lower termination, but this is considered negligible in view of the very low field there ($B^2/B^2_{\mathrm{peak}} < 0.1$). The total (hysteresis + coupling) energy loss $E_{\mathrm{cond}}$ (J) of the main winding conductor can then be obtained by integrating $Q_{\mathrm{WIND}}$ in time; the integration of $Q_{\mathrm{IJ}}$ gives the energy loss $E_{\mathrm{IJ}}$ (J) of the IJ and the integration of $Q_{\mathrm{WIND}} + Q_{\mathrm{IJ}} + Q_{\mathrm{BUS}}$ gives the total loss $E_{\mathrm{tot}}$ (J).

The evolution of the enthalpy differences $\Delta h$ needed for the calorimetric estimation above is shown in figure 7 for the case of a typical 4 T CSMC dump. It may be noted that, while $\Delta h \approx 0$ both at the beginning and at the end of the transient in the case of the facility sensors (TCin and TCout), $\Delta h \neq 0$ when we consider any combination based on conductor thermometers. Also, for the same pair of sensors, $\Delta h_{\mathrm{initial}}$, at the beginning of the transient, is different from $\Delta h_{\mathrm{final}}$, at the end, with the only exception being $h$(PT_BB, T05H) − $h$(PT_BB, TIJin), which may be related to the fact that the field correction for T05H is less significant.

To address these issues we correct T04H and T05H in such a way that $h$(PT_out, T04H) − $h$(PT_in, TCin) + $g\Delta z_{04-\mathrm{in}}$ and $h$(PT_BB, T05H)−$h$(PT_BB, TIJin) vanish *at a given time* $t = t^{\#}$ in the absence of sources (the so-called 'enthalpy offset'). The choice of $t^{\#}$ is delicate for T04H, as the corresponding $\Delta h$ is different before and after the dump, see above. If we use as offset $\Delta h_{\mathrm{final}}$, we notice that [$h$(PT_out, T04H) − $h$(PT_in, TCin) + $g\Delta z_{04-\mathrm{in}}$] becomes > 0 before the dump, therefore the AC loss will be somewhat overestimated and this will constitute the *upper* bound of our estimate for $Q_{\mathrm{WIND}}$.

We now consider an alternative estimate of the losses in the winding, using only the inlet/outlet temperatures and assuming the IJ losses split equally between the two IJ halves, namely

$$Q^{\mathrm{split}}_{\mathrm{WIND}} = (\mathrm{d}m/\mathrm{d}t)_{\mathrm{cond}}[h(\mathrm{PT\_out, TCout}) - h(\mathrm{PT\_in, TCin}) + g\Delta z_{\mathrm{out-in}}] - \tfrac{1}{2}Q_{\mathrm{IJ}}.$$

Although $Q^{\mathrm{split}}_{\mathrm{WIND}} = Q_{\mathrm{WIND}}$ exactly if the IJ losses are split equally between the two IJ halves, we can use $Q^{\mathrm{split}}_{\mathrm{WIND}}$ to get a *lower* bound for $Q_{\mathrm{WIND}}$ as follows. Also the estimate of the IJ losses suffers of the uncertainty on the T04H correction. However, in this case we can offset the enthalpies both at the end of the transient (as suggested above for the winding) and at the beginning of the transient, as done in [14]. In the latter case, the issue of when to cut the integration time can be solved by using the time when the enthalpy difference vanishes on the other (busbar) side of the IJ, which is not affected by the problem of the different $\Delta h$ between the beginning and end of the transient, as discussed above. We then use the upper bound for $Q_{\mathrm{IJ}}$ in the expression of $Q^{\mathrm{split}}_{\mathrm{WIND}}$ above, which then provides a *lower* bound to the main winding losses.

The resulting calorimetric estimates of the AC loss for the reference CSMC exponential dumps from 4 T ($\tau_{\mathrm{dump}} \sim 5.6$ s), with $I_{\mathrm{PFCI}} = 0$ kA, are presented in table 2. In order to separate coupling and hysteresis losses, recent results of strand measurements performed at CERN were used [24] (as a reference, a model based on classical formulae [25] with effective filament diameter $d_{\mathrm{eff}} = 9.8$ $\mu$m gives ∼500 J, roughly independent of cycling and not too far from the CERN measurements). The $n\tau$ range was computed using min $(E_{\mathrm{coupl}}) = \min(E^{\mathrm{split}}_{\mathrm{WIND}}) - E_{\mathrm{hyst}}$, where $E^{\mathrm{split}}_{\mathrm{WIND}}$ results from the time integration of $Q^{\mathrm{split}}_{\mathrm{WIND}}$, and max $(E_{\mathrm{coupl}}) = E_{\mathrm{WIND}} - E_{\mathrm{hyst}}$, respectively.

It was seen that the conductor losses increased with cycling until quench events brought the conductor back or close to virgin values, but then values close to those before quench was recovered again after further cycling. A similar phenomenon was observed earlier in measurements with the Twente press, with a noticeable increase of the interstrand contact resistance and consequently a decrease of the coupling loss [26]. Although speculative, it is not unlikely that a quench event leads to a small mechanical distortion of the

**Table 2.** AC losses in CSMC exp dumps from 4 T ($\tau_{\text{dump}} \sim 5.6$ s, $I_{\text{PFCI}} = 0$ kA).

| Run # (# of cycles) | $E_{\text{WIND}}$ (J) | $E_{\text{IJ}}$ (J) | $\min(E^{\text{split}}_{\text{WIND}})$ (J) | $M_{\text{IJ-axial}}$ (au) | $M_{\text{IJ-radial}}$ (au) | $E_{\text{hyst}}$ (J) | $n\tau$ (ms) |
|---|---|---|---|---|---|---|---|
| 054 (before cyclic tests) | 1060 | 1305–1295 | 840 | 16.5 | 9.22 | 600 | 9–17 |
| 063 (∼430) | 1530 | 1730–1540 | 1495 | 16.2 | 9.63 | 655 | 32–33 |
| 066 (∼1000) | 1610 | 1795–1455 | 1295 | | | 655 | 24–36 |
| 069 (∼1700) | 1890 | 1715–1455 | 1650 | | | 655 | 37–46 |
| 071 (∼2800) | 2075 | 1695–1440 | 1810 | | 9.82 | 655 | 43–53 |
| 074 (∼4000, before quench test) | 1940 | 1750–1450 | 1580 | | 10.03 | 655 | 35–48 |
| 119 (after quench test) | 940 | 1560–1350 | 670 | | | 610 | 2–12 |
| 134 (∼9000, before high field quench) | 2225 | 1860–1490 | 1950 | | | 655 | 49–59 |

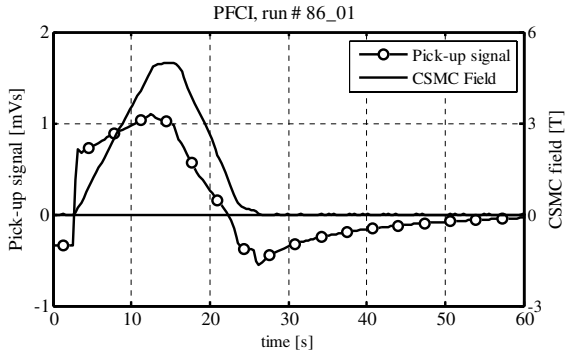


**Figure 8.** Time-integrated pick-up signal and trapezoidal CSMC field pulse.

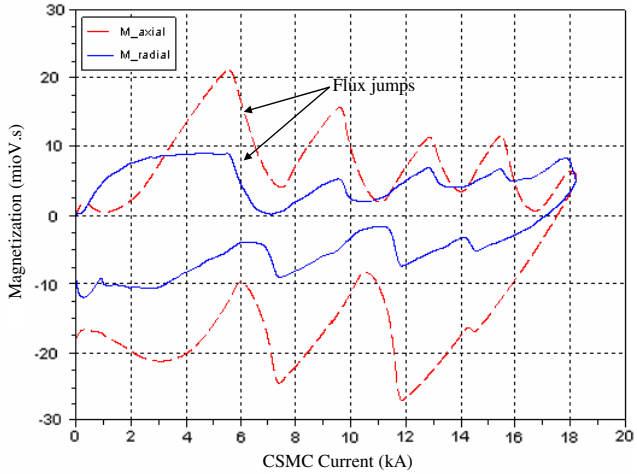


**Figure 9.** PU Magnetization loops of the IJ during a CSMC trapezoidal field pulse at 18.2 kA: axial direction (dashed) and radial direction (solid).

strand locations in the cable, eventually changing the spatial interstrand contacts leading to higher contact resistances until further cycling again causes a decrease.

In view of the fact that the cycling test was stopped at ∼9000 cycles as planned, because of time restrictions in the duration of the campaign, we cannot say if the losses are already saturating or could still increase, as observed in the case of the short-sample tests in the Twente press.

### *4.2. Evaluation of conductor and IJ losses from magnetization measurement (PU coils)*

The signal from the conductor PU coil may be useful for confirmation of the conductor magnetization and thus the conductor AC losses in terms of coupling and hysteresis components. For the coupling loss, the multiple time constants' nature [22] associated with the complex cabling pattern in large CICCs may be the explanation of the long decay time of the coupling currents at the end of a trapezoidal run. In figure 8 the PU signals from sensor IPF_VC_01 (middle of the winding) and the CSMC field are plotted versus time. When the CSMC trapezoidal field pulse is completed, there is still a significant decay of the magnetization, interpreted as a decay of coupling currents associated with large loops. A similar decay occurs at the end of the rise of the field but the plateau is too short (≈3 s) to allow a full relaxation of the induced currents. The low pass filtering of the PU coil signals by the PFCI instrumentation is probably too severe for the higher harmonics to allow detection of short time constants (around several tens of ms). A simple two-time-constant fit to the decaying signal after the field pulse gives time constants of about 2 s and about 12 s.

The plots in figure 9 show the IJ magnetization according to the axial and radial field directions (with respect to the coil) during a CSMC trapezoidal field run: the axial field amplitude is 3.6 T and the radial field amplitude is 1.2 T; the ramping up and down times are both equal to 17 s. Note that the magnetization values at maximum current are uncertain because of the too short plateau duration. One can clearly see in this figure a series of so-called 'flux jumps', i.e. fast decreases of the magnetization which likely correspond to overload and local quench of strands inside the joint due to high screening currents induced by the field change in the joint. This phenomenon was anticipated from measurements performed on sub-size joints. PU coils were used to diagnose these instabilities, which cannot be identified by calorimetry because of the too short timescale of these sudden events; indeed, only a decrease of the losses when increasing the ramp rate can be measured by calorimetry [27].

Although the modeling is not yet able to compute directly the energy loss from the areas $M_{\text{IJ}}$ of the magnetization curves, the proportionality of these areas with the energy loss already allows relative estimations between runs (see table 2), to be compared with the calorimetric estimates. It should be noted that there is some disagreement in the variation of IJ AC losses from virgin to cycled, with respect to the calorimetric

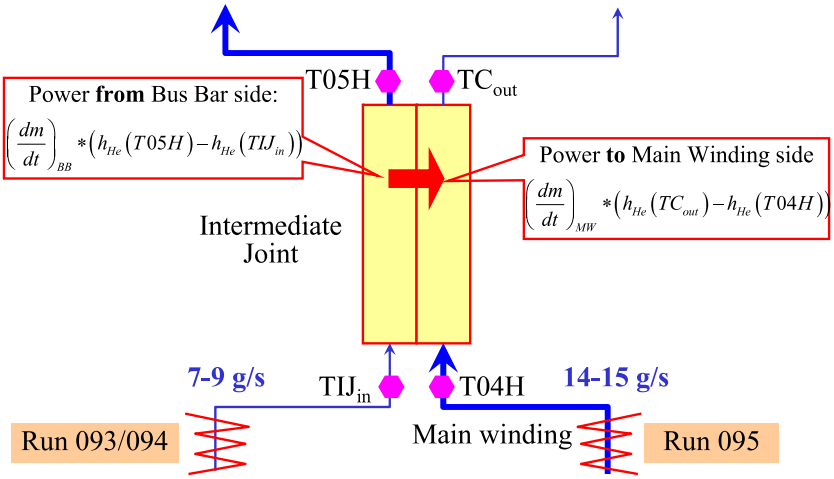


**Figure 10.** Set-up for the measurement and assessment of heat transfer through the IJ.

estimates, see above, but both estimates then saturate during cycling.

## 5. IJ resistance and heat transfer

The IJ resistance has been evaluated calorimetrically in different runs, with different transport current and different background field. At zero external field and $I_{\mathrm{PFCI}} = 52$ kA (run #015-01), the computed resistance turned out to be ∼1 nΩ on the main winding side and ∼1.4 nΩ on the upper busbar side, giving ∼2.4 nΩ in total, which is much lower than the value measured on the short sample and in good agreement with the electrical estimation given in [7]. The similar significant reduction with respect to the short sample values is also estimated for the bottom termination (which underwent as well as the IJ an improved manufacturing procedure for the PFCI), whereas the top termination resistance is estimated to be relatively high (∼6 $n\Omega$).

Also the heat transfer between two jointed conductors through the joint itself has been the subject of other investigations in the past, for different joint types and geometries, see [28, 29]. The problem is of some interest because, in view of the large mass/area of Cu, the joint is typically a relatively good heat exchanger, but the absence of temperature differences between the two jointed conductors cannot always be guaranteed.

The heat transfer in the IJ was measured in three runs by using selectively either the resistive heaters upstream of the busbar channel (runs 93-01 and 94-01) or the resistive heater upstream of the main winding (run 95-01), in a series of steps allowing steady states to be reached with different operating conditions. In principle, the resulting global heat transfer coefficient $H$, which assumes constant properties (e.g. $c_p$) and negligible axial heat conduction in the joint, could be straightforwardly evaluated calorimetrically starting from the measured temperatures upstream and downstream of the IJ in the two jointed conductors and applying the following formulae:

$$Q_{\mathrm{transfer}} = H A \Delta T_{lm}$$

**Table 3.** Contributions to the IJ energy balance in different runs.

| Run # | Power from busbar (W) | Power to main winding (W) |
|---|---|---|
| 093-01 | 0.69 | 1.27 |
| | 1.71 | 2.77 |
| | 3.04 | 5.16 |
| 094-01 | 0.13 | 0.62 |
| | 0.77 | 2.40 |
| | 1.43 | 4.40 |
| 095-01 | −2.55 | −2.47 |
| | −5.65 | −5.84 |
| | −9.17 | −10.16 |

$$\Delta T_{lm} = \frac{(\mathrm{T04H} - \mathrm{TC_{out}}) - (\mathrm{TIJ_{in}} - \mathrm{T05H})}{\ln \frac{(\mathrm{T04H} - \mathrm{TC_{out}})}{(\mathrm{TIJ_{in}} - \mathrm{T05H})}}$$

where $Q_{\mathrm{transfer}}$ is the power transferred across the joint, $A$ is the heat transfer area and the mean logarithmic temperature difference $\Delta T_{lm}$ refers to a co-current heat exchanger, as is the case in the PFCI IJ.

However, it turns out following the strategy highlighted in figure 10, which is based on a similar approach as described above for the calorimetry of AC losses, that only run 95-01 allows a sufficiently accurate reconstruction of the energy balance through the joint (i.e. the condition that the power released by the heated conductor equals the power received by the non-heated conductor, both being equal to $Q_{\mathrm{transfer}}$), see table 3. The fact that T04H-TCin increases (not shown) even when, as in runs 093-01 and 094-01, the main winding side is only indirectly heated, possibly due to heat conduction from the IJ, is a good candidate to explain the inadequacy of the above calorimetric estimate in these two cases. Therefore, we shall restrict our considerations in the following to run 95-01.

The results of our analysis are summarized in table 4. The global heat transfer coefficient HA ∼6 ± 1 W K$^{-1}$ for this run, with a slightly increasing trend likely related to slightly increasing Prandtl (and Reynolds) number at increasing $Q_{\mathrm{heater}}$. It may be noted that the heat transfer efficiency $Q_{\mathrm{transfer}}/Q_{\mathrm{heater}}$ is remarkably constant at ∼10%, independent of the heating

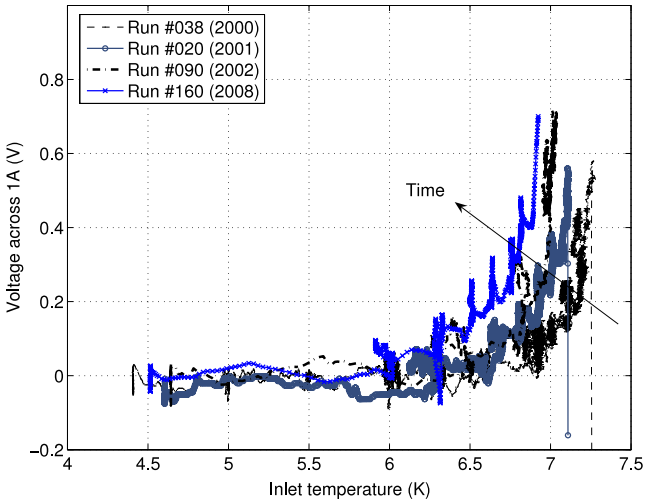


**Figure 11.** Comparison of measured voltage–temperature characteristics of CSMC conductor 1A in different test campaigns over the last eight years.

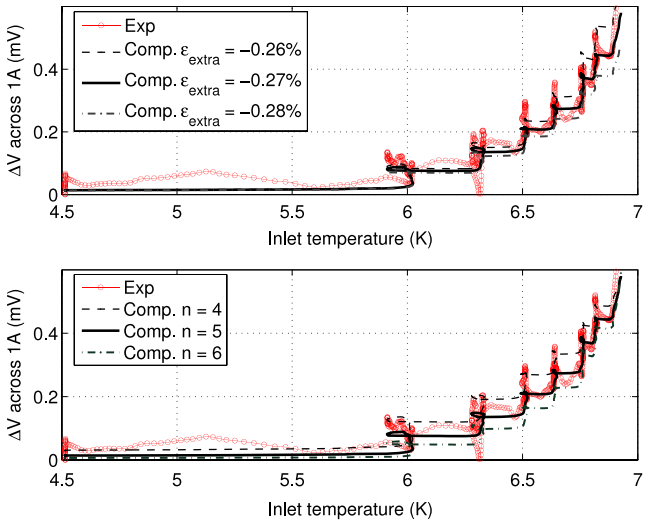


**Figure 12.** Performance assessment of CSMC conductor 1A at the end of the PFCI test.

**Table 4.** Heat transfer efficiency of the IJ in different operating conditions (run 095-01).

| $Q_{\text{transfer}}$ (W) | $Q_{\text{heater}}$ (W) | $\Delta T_{lm}$ (K) | HA (W K$^{-1}$) |
|---|---|---|---|
| 2.5 | 23.5 | 0.475 | 5.3 |
| 5.7 | 58.9 | 0.906 | 6.3 |
| 9.7 | 105.0 | 1.35 | 7.2 |

power level; this is expected from simple heat exchanger theory for this fluid and for the given mass flow rates [30]. In comparison with the previous assessment of the SS-FSJS joint, operating also as the co-current heat exchanger [28], the heat transfer efficiency turns out to be smaller in the case of the PFCI IJ. This picture appears consistent with the larger electrical resistance of the latter, if compared to the former (0.84 nΩ–1.34 $n\Omega$ @ 2 T and 7 T, respectively, quoted in [31]).

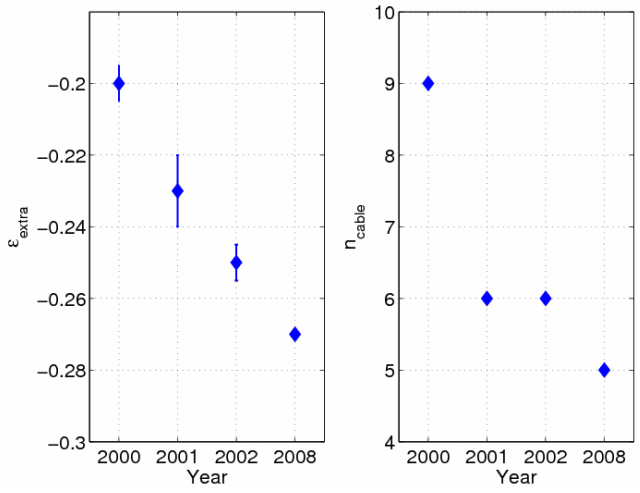


**Figure 13.** Degradation of performance of CSMC conductor 1A over the years.

## 6. DC performance of the CSMC 1A conductor

As for all other ITER insert coils [2, 4, 5], the standard $T_{\text{CS}}$ test of the CSMC conductor 1A at $I_{\text{CSMC}} = 46$ kA was conducted at the end of the PFCI test campaign. The result of this test in terms of measured V–Tin characteristic is reported in figure 11 and compared to the similar characteristics measured during the previous test campaigns (CSIC in 2000, TFCI in 2001, ALI in 2002). It may be seen by eye that some degradation occurred during the series of campaigns and in particular also between the last CSMC test in 2002 and the PFCI test. However, in the case of the PFCI test the CSMC current was raised only a few times up to 32 kA (50% of $I \times B$) and only once at 46 kA. There was therefore no real 'cycling effect' on the CSMC, compared to the previous tests, so that the cause of this last degradation is somewhat obscure.

In order to analyze and quantify the degradation, the same approach was applied, based on the M&M code [32], which was already used for the 2000–2 campaigns [33]. Two free parameters—the conductor $n$ index and the additional (typically compressive) strain $\varepsilon_{\text{extra}}$ on the filaments, needed to reproduce the conductor performance, were used. A parametric study was thus conducted, giving as optimum $n \sim 5$ and $\varepsilon_{\text{extra}} \sim -0.27\%$, see figure 12. If compared to previous degradation assessments, it can be seen that the degradation in both parameters has also continued with the PFCI test, see figure 13.

Summarizing, with respect to the first test campaign in 2000, the CSMC (conductor 1A) performance appears to be slowly but steadily degrading with time:

- $T_{\text{CS}}$@46 kA, 13 T decreased from ~7.21–7.30 K to ~6.92 K →~ 0.3–0.4 K loss;
- $n_{\text{conductor}}$ decreased from 9 to 5.

## 7. Conclusions and perspective

The good overall results of the PFCI conductor DC tests are being interpreted by the models suggesting less than 0.15 K deviation from the ultimate performance expectation based on the single-strand properties. The improvement with respect to the short sample is explained by improved uniformity of the current in the high field area.

Calorimetric analysis of AC losses qualitatively confirms the trends of conductor $n\tau$ with cycling as observed on the PFCI short sample tested in the Twente press. The estimated upper bound after 9000 cycles is $n\tau \sim 60$ ms, which is well below the allowed 100 ms.

The low resistance ($\sim$2.4 $n\Omega$ @ 0 T) and heat transfer efficiency ($\sim$10%) of the PFCI Intermediate Joint have been assessed calorimetrically.

The slow but steady degradation of the CSMC (conductor 1A) performance, already noted during the tests of previous ITER insert coils, appears to be confirmed by the test performed during the PFCI test campaign.

Only two pulse current tests (at 5 kA $s^{-1}$) were performed on the PFCI. They showed some significant degradation of the conductor performance compared to its DC performance, which can be related to the so-called ramp-rate limitation (RRL). However, these two tests did not give fully consistent results regarding the associated quench temperature. Unfortunately, due to an operating voltage limit of 1 kV [9], no exhaustive tests could be carried out on this topic. However, this is not considered by ITER IO as a cause of major concern for the PF conductor design because the pulsed operation range for the PF coils is far from this possible RRL [34].

Stability and quench propagation tests, as well as the degradation of the IJ DC performance, are still the subject of analysis and the results will be reported elsewhere.

## Acknowledgments

The participation of RZ, BL and LSR in the PFCI test was financially supported by EURATOM mobility. The kind hospitality of JAEA Naka, Japan, during the test period is also gratefully acknowledged. The work of RZ and LSR was also partially financially supported by the Italian Ministry for University and Research (MiUR) and LSR is a grateful recipient of a fellowship 'Giovani ricercatori' of Politecnico di Torino. EPAvL is partially financially supported by the University of Twente. MB is partially financially supported by CRPP. Both MB and EPAvL were also supported by a Marie Curie trainee fellowship. ITER IO partially financially supported the PFCI test. This report was prepared as an account of work for the ITER Organization. The Members of the Organization are the People's Republic of China, the European Atomic Energy Community, the Republic of India, Japan, the Republic of Korea, the Russian Federation and the United States of America. The views and opinions expressed herein do not necessarily reflect those of the Members or any agency thereof. Dissemination of the information in this paper is governed by the applicable terms of the ITER Joint Implementation Agreement.

## References

[1] Tsuji H *et al* 2001 Progress of the ITER central solenoid model coil program *Nucl. Fusion* **41** 645
[2] Martovetsky N *et al* 2002 Test of the ITER central solenoid model coil and CS insert *IEEE Trans. Appl. Supercond.* **12** 600
[3] Ulbricht A *et al* 2005 The ITER toroidal field model coil project *Fusion Eng. Des.* **73** 189
[4] Okuno K *et al* 2003 Test of the NbAl insert and ITER central solenoid model coil *IEEE Trans. Appl. Supercond.* **13** 1437
[5] Martovetsky N *et al* 2003 Test of the ITER TF insert and central solenoid model coil *IEEE Trans. Appl. Supercond.* **13** 1441
[6] Mitchell N *et al* 2008 The ITER magnet system *IEEE Trans. Appl. Supercond.* **18** 435
[7] Bessette D *et al* 2008 Test results from the PF conductor insert coil and implications for the ITER PF system *ASC (Chicago, IL, Aug.)*
[8] Baker W *et al* 2007 Manufacture of the poloidal field conductor insert coil (PFCI) *Fusion Eng. Des.* **82** 1567
[9] Nunoya Y *et al* 2008 Installation and Test Programme of the ITER poloidal field conductor insert (PFCI) in the ITER test facility at JAEA Naka *ASC (Chicago, IL, Aug.)*
[10] Zanino R *et al* 2005 Preparation of the ITER poloidal field conductor insert (PFCI) test *IEEE Trans. Appl. Supercond.* **15** 1346
[11] Bruzzone P *et al* 2005 Test results of the ITER PF insert conductor short sample in SULTAN *IEEE Trans. Appl. Supercond.* **15** 1351
[12] Zanino R *et al* 2006 Implications of NbTi short-sample test results and analysis for the ITER poloidal field conductor insert (PFCI) *IEEE Trans. Appl. Supercond.* **16** 886
[13] Mitchell N 2009 private communication
[14] Zanino R *et al* 2008 EU Contribution to the Test and Analysis of the ITER poloidal field conductor insert (PFCI) *Proc. 2008 IAEA FEC (Geneva)*
[15] Ciazynski D *et al* 2005 DC performances of ITER NbTi conductors: models versus measurements *IEEE Trans. Appl. Supercond.* **15** 1355
[16] Zanino R *et al* 2007 Predictive analysis of the ITER poloidal field conductor insert (PFCI) test program *IEEE Trans. Appl. Supercond.* **17** 1353
[17] Zani L *et al* 2005 Jc(T, B) characterization of NbTi strands used in ITER PF-relevant insert and full-scale sample *IEEE Trans. Appl. Supercond.* **15** 3506
[18] Van Lanen E P A *et al* 2009 Simulation of the ITER poloidal field coil insert DC performance with a new model *Fusion Eng. Des.* **84** 1912–5
[19] Ilyin Y *et al* 2006 Interpretation of conduit voltage measurements on the poloidal field insert sample using the CUDI-CICC numerical code *Cryogenics* **46** 517
[20] Ilyin Y *et al* 2005 Effect of cyclic loading and conductor layout on contact resistance of full-size ITER PFCI conductors *IEEE Trans. Appl. Supercond.* **15** 1359
[21] Bruzzone P *et al* 2006 A critical review of coupling loss results for cable-in-conduit conductors *IEEE Trans. Appl. Supercond.* **16** 827
[22] Nijhuis A *et al* 1995 Study on the coupling loss time constants in full size Nb3Sn CIC model conductors for fusion magnets *Adv. Cryog. Eng.* B **42** 1281
[23] Zapretilina E 2008 AC loss in PFIC and short samples. Application to the ITER PF coils *PF Insert Coil Workshop (JAEA, Naka, Oct.)*
[24] Bottura L 2008 Analysis of AC loss in the PFIC by calorimetry *PF Insert Coil Workshop (JAEA, Naka, Oct.)*
[25] Lacroix B *et al* 2008 Predictive study of the poloidal field coil insert behaviour under pulsed current tests *J. Phys.: Conf. Ser.* **97** 012201
[26] Nijhuis A *et al* 2004 Change of interstrand contact resistance and coupling loss in various prototype ITER NbTi conductors with transverse loading in the Twente cryogenic cable press up to 40 000 cycles *Cryogenics* **44** 319

[27] Zani L *et al* 2003 Manufacture and test of NbTi subsize joint samples for the ITER poloidal field coils *IEEE Trans. Appl. Supercond.* **13** 1460
[28] Zanino R and Savoldi L 2000 Test and modeling of heat generation and heat exchange in the full size joint sample *Proc. 18th Int. Cryogenic Engineering Conf.* p 363
[29] Savoldi L *et al* 2000 Tests and simulation of thermal-hydraulic transients in the US prototype joint sample *Int. J. Mod. Phys.* B **14** 3183
[30] Incropera F P and De Witt D P 2002 *Fundamentals of Heat and Mass Transfer* (New York: Wiley)
[31] Ciazynski D *et al* 2000 Large superconducting conductors and joints for fusion magnets: from conceptual design to test at full size scale *Paper FTP1/14, FEC*
[32] Savoldi L and Zanino R 2000 M&M: multi-conductor mithrandir code for the simulation of thermal-hydraulic transients in superconducting magnets *Cryogenics* **40** 179
[33] Zanino R *et al* 2003 Analysis and interpretation of the full set (2000–2002) of Tcs tests in conductor 1A of the ITER central solenoid model coil *Cryogenics* **43** 179
[34] Mitchell N 2009 Conclusions from PF insert tests *PF Design Review Mtg (Cadarache, Jan.)* ITER_D_2N7FEJ v1.0